symmetry

IMPACT FACTOR 2.940

CITESCORE 4.3

Article

QCD Matter and Phase Transitions under Extreme Conditions

Mei Huang and Pengfei Zhuang

Special Issue

Heavy-Ion Collisions and Multiparticle Production

Edited by

Prof. Dr. Qun Wang, Prof. Dr. Zuotang Liang and Prof. Dr. Enke Wang

MDPI

https://doi.org/10.3390/sym15020541

symmetry

MDPI

Article

QCD Matter and Phase Transitions under Extreme Conditions †

Mei Huang [1,*,‡] and Pengfei Zhuang [2,*,‡]

[1] School of Nuclear Science and Technology, University of Chinese Academy of Sciences, Beijing 100049, China
[2] Department of Physics, Tsinghua University, Beijing 100084, China
* Correspondence: huangmei@ucas.ac.cn (M.H.); zhuangpf@tsinghua.edu.cn (P.Z.)
† This work is in memory of Professor Lianshou Liu.
‡ These authors contributed equally to this work.

Abstract: The interplay of chiral dynamics and gluodynamics plays an essential role in the nonperturbative QCD region, and the chiral phase transition and deconfinement phase transition are the main topics of QCD phase transitions under extreme conditions, e.g., finite temperature and/or baryon density, strong magnetic fields, and fast rotation. We briefly introduce our own recent progress from the theoretical side on QCD phase transitions and phase diagrams under extreme conditions related to the early universe, compact stars, and heavy-ion collisions.

Keywords: QCD phase transitions; chiral dynamics; gluodynamics

check for updates

Citation: Huang, M.; Zhuang, P. QCD Matter and Phase Transitions under Extreme Conditions. *Symmetry* **2023**, *15*, 541. https://doi.org/10.3390/sym15020541

Academic Editor: Dubravko Klabučar

Received: 31 December 2022
Revised: 8 February 2023
Accepted: 15 February 2023
Published: 17 February 2023

Copyright: © 2023 by the authors. Licensee MDPI, Basel, Switzerland. This article is an open access article distributed under the terms and conditions of the Creative Commons Attribution (CC BY) license (https://creativecommons.org/licenses/by/4.0/).

1. Introduction

Quarks and gluons are fundamental building blocks of visible matter, and their interaction is described by quantum chromodynamics (QCD) [1,2]. QCD matter (here we mean quark matter) (Although nuclear matter should be considered as one type of QCD matter, in this paper, in most cases, QCD matter refers to matter consisting of quarks and gluons, i.e., quark matter) existed at around 10 microseconds in the early universe [3] and exists inside the core of compact stars [4,5], and it can be created through relativistic heavy-ion collisions [6]. Thus, understanding quark matter's properties and QCD phase transitions under extreme conditions is of special interest in investigating the evolution of the universe, exploring the structure of compact stars, and understanding observable heavy-ion collisions [7,8].

The interplay of chiral dynamics and gluodynamics plays an essential role in the nonperturbative QCD region and determines the QCD phase structures. The chiral phase transition and deconfinement phase transitions are two important phase transitions well defined in two extreme quark mass limits, respectively. The chiral phase transition is well defined in the chiral limit characterized by the order parameter of the chiral condensation of light flavors $\langle\bar{\psi}\psi\rangle$ and the deconfinement phase transition, which is characterized by the order parameter of the Polyakov-loop $\langle L\rangle$ in the heavy quark mass limit.

At high temperatures, QCD phase transitions can be calculated by using a lattice. As shown in Figure 1 taken from [9], the QCD phase transitions are flavor- and quark-mass-dependent [7–10]. For the three-flavor massless quark limit or three light quarks, the chiral phase transition is of first-order at the critical temperature around $T_c^\chi = 155\,\mathrm{MeV}$, and in the case of a two-flavor degenerate massless u, d quark and a relative heavy s quark, the chiral phase transition is of second-order around the critical temperature $T_c^\chi = 175\,\mathrm{MeV}$; when the u, d quark has a small current quark mass, the chiral phase transition will become a cross-over. The lattice calculation [11] shows that, with the physical quark mass, the chiral phase transition at finite temperature in the hot early universe is not a real phase transition, but a smooth cross-over. When the quark mass is heavy and becomes infinity, QCD becomes the pure gauge theory of $SU(3)_c$, and lattice gives the first-order deconfinement phase transition from the Polyakov-loop-order parameter at the critical temperature

around $T_c^d = 270\,\mathrm{MeV}$. However, it is not known how the chiral dynamics interplay with gluodynamics and affect the phase transitions.

The properties of dense QCD matter are important to understand the structure of compact stars, which is related to heavy-ion collisions at low collision energy; see the review article [6]. The lattice calculation is still facing the sign problem at finite baryon chemical potential, and some progress has been made in exploring the phase transitions by using the Taylor expansion of μ_B/T [12–15] and using the simulation of imaginary chemical potential(s) [16]. Through symmetry analysis [17,18] and predictions from effective chiral models, e.g., the Nambu–Jona–Lasinio (NJL) model [19,20] and its Polyakov-loop improved version [21–23], the Polyakov-loop linear sigma model and hadron resonance gas model [24–26], and the Dyson–Schwinger equations (DSEs), which considers quarks and gluons' degrees of freedom [27,28], as well as the five-dimensional holographic QCD model [29], which can take into account chiral dynamics and gluodynamics, etc., it is believed that, in the case of two flavors, the chiral phase transition becomes first order at high baryon chemical potential, and the end point along the first-order phase transition line is called the critical end point (CEP). The search for the QCD CEP is one of the main goals of the Beam Energy Scan (BES) program for relativistic heavy-ion collisions (RHICs), the future program at the Facility for Antiproton and Ion Research (FAIR) at Darmstadt, Germany, and the Nuclotron-based Ion Collider Facility (NICA) at JINR, Dubna.

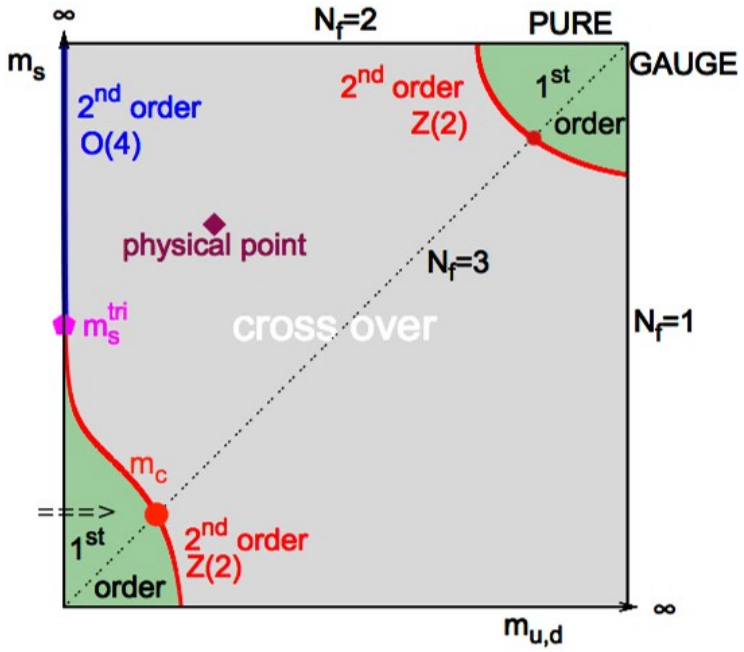

Figure 1. Lattice results on QCD phase diagram at high temperature with a degenerate u, d quark with $m_u = m_d$ and a strange quark with mass m_s. The figure is taken from [9].

Through non-central heavy-ion collisions, the strong magnetic field with the magnitude of 10^{18-19} Gauss and angular momentum of QGP at a range of 10^4–$10^5\hbar$ can be generated [30–35]. Both the magnetic field and angular momentum will polarize the medium, thus changing the properties of QCD matter.

In this short overview, we summarize our own contribution from the theoretical side on the recent progress of QCD phase transitions and QCD matter properties under extreme conditions related to the early universe, compact stars, and heavy-ion collisions.

2. Imprints of QCD Epoch in the Early Universe

The observation of GW signals by LIGO and the Virgo Collaboration [36] 100 years after their prediction [37,38] opens an exciting era for cosmology. Except that the GWs can

be produced through compact binary merges and inspirals, it has also been predicted that the primordial stochastic GW could be produced in the very early stages of the universe through a strong first-order phase transition (FOPT) during inflation, Grand Unified Theory (GUT) symmetry breaking, electroweak phase transition (EWPT) [39–46], as well as QCD phase transition [3,47–50]. GWs carry unique imprints of the early universe about these phase transitions on the cosmic microwave background [51–54]. Except the GWs, another interesting topic during the QCD epoch is the generation of the primordial black holes (PBHs) predicted 50 years ago [55–57], which are possible candidates for dark matter. In the QCD phase transitions around the temperature of $T\sim$200 MeV, one would expect the PBH mass to show a peak in the solar mass range [58–60].

In the Minimal Standard Model (SM), the EWPT is well known as a cross-over [39], and it can be a strong FOPT [61] when new physics is considered such as the singlet extension of the SM and two-Higgs-doublet models [40–46]. Similarly, though the lattice QCD predicted that, for a physical mass with $m_u = m_d << m_s$, the system would experience a cross-over in the QCD epoch, there are still other physical conditions in the QCD epoch, and the system experiences a strong FOPT. For example, the pure gluon system might appear in the temperature region below the EWPT, and it exhibits a strong FOPT, as shown by the lattice results [10], as well as the holographic QCD description [62–64], and possible glueball dark matter was investigated in [65,66]. Another interesting FOPT in the QCD epoch is related to the sphaleron transition, which induces chirality imbalance and the violation of $\mathcal{P}$- and $\mathcal{CP}$-symmetry, and the gravitation wave and primordial black hole induced by chirality imbalance under a magnetic field were investigated in [67].

QCD has an important $U(1)_A$ axial symmetry, which is anomalously broken by quantum effects, and the $U(1)_A$ problem or the puzzle of the η and η' mass difference was resolved by the instantons proposed by 't Hooft [68,69]. The chiral anomaly is closely related to the non-trivial topological QCD θ vacuum structure characterized by the integer Chern–Simons number $N_{cs} = \frac{g^2}{32\pi^2}\int \mathrm{d}^4x\, F^a_{\mu\nu}\tilde{F}^{\mu\nu}_a$ [70]. Different Chern–Simons sectors are connected through instanton and sphaleron transitions at zero and finite temperatures, respectively. The Chern–Simons number change through the axial anomaly induces the chirality imbalance between the right-handed and left-handed quarks, $N_5 = N_R - N_L = \int d^4x \partial_\mu j^\mu_5 = -2N_f N_{cs}$, represented by an axial chemical potential μ_5, and results in a violation of $\mathcal{P}$- and $\mathcal{CP}$-symmetry [71–74]. It has been proposed in non-central heavy-ion collisions with a strong magnetic field that this chirality imbalance and local $\mathcal{P}$- and $\mathcal{CP}$-symmetry violation might produce the chiral magnetic effect (CME) [75–77], i.e., parity-odd domains lead to the charge separation of quarks, which has been one of the main goals for RHICs.

Based on the instanton–anti-instanton molecule picture [78–80], in [81,82], it was shown that an effective axial chemical potential μ_5, which describes the chirality imbalance, can be dynamically induced by a repulsive axial vector interaction. The Lagrangian density takes the form:

$$\mathcal{L} = \bar{\psi} i\gamma_\mu D^\mu \psi + G_S\left[(\bar{\psi}\psi)^2 + \left(\bar{\psi} i\gamma^5 \tau\psi\right)^2\right] - G_V(\bar{\psi}\gamma^\mu\psi)^2 - G_A\left(\bar{\psi}\gamma^\mu\gamma^5\psi\right)^2 .$$

where τ is the Pauli matrices in the flavor space and G_S, G_V, and G_A are the coupling constants in the scalar, the vector, and the axial vector channels. Quarks with electric charge q_f couple to a magnetic field $\vec{B} = (0,0,B)$ with $A_\mu = (0,0,-xB,0)$ through the covariant derivative $D_\mu = \partial_\mu - iq_f A_\mu$. Introducing the quark condensate $\sigma = -2G_S\langle\bar{\psi}\psi\rangle$, which is the the order parameter of the chiral phase transition and the dynamical chiral chemical potential $\mu_5 = -2G_A\langle\bar{\psi}\gamma^0\gamma^5\psi\rangle$ describing the chirality imbalance between left- and right-handed quarks, one can derive the thermodynamical potential:

$$\Omega = \frac{\sigma^2}{4G_S} - \frac{\mu_5^2}{4G_A} - N_c \sum_{u,d} \frac{|q_f B|}{2\pi} \sum_{s,k} \alpha_{sk} \int_{-\infty}^{+\infty} \frac{\mathrm{d}p_z}{2\pi} f_\Lambda^2(p) \omega_{sk}(p) - 2N_c T \sum_{u,d} \frac{|q_f B|}{2\pi} \sum_{s,k} \alpha_{sk} \int_{-\infty}^{+\infty} \frac{\mathrm{d}p_z}{2\pi} \ln\left(1 + e^{-\beta\omega_{sk}(p)}\right). \quad (1)$$

where the eigenvalues of the Dirac operator are $\omega_{sk} = \sqrt{\sigma^2 + (p + s\mu_5 \mathrm{sgn}(p_z))^2}$ and the spin degeneracy factor is $\alpha_{sk} = 1 - \delta_{k,0} + \delta_{k,0}\delta_{s,\mathrm{sgn}(q_f B)}$ with $s = \pm 1$. Then, we can solve the phase transition from the thermodynamical potential, and the results are shown in Figure 2a, which shows that the phase transition of the chirality imbalance is of first order with $r_A = -0.3, -0.5, -0.8$ at $B = 0$. The FOPT will induce GWs and generate PBHs. The bounce solution and bubble nucleation temperature of this FOPT are solved to obtain the strength parameter α and the inverse duration time β/H, which are essential to calculate the gravitational wave power spectra in [67]. The results are shown in Table 1.

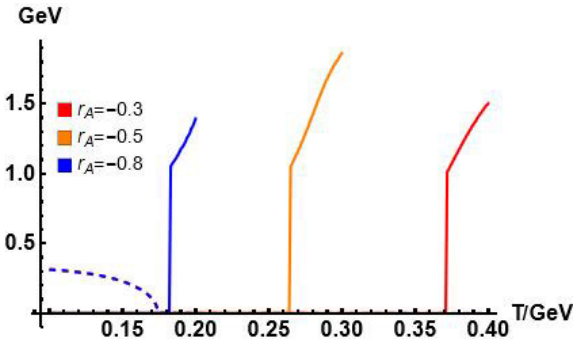

(**a**) $\mu 5$ (lines) and σ (dashed lines) as a function of T at $eB = 0$.

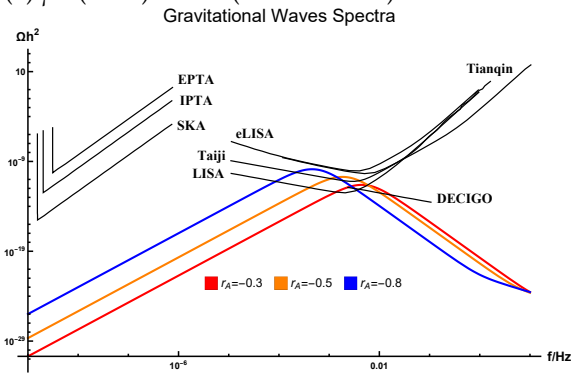

(**b**) Gravitational wave spectra.

Figure 2. (**a**) The chiral condensate σ (dashed lines) and the dynamically induced chiral chemical potential μ_5 (lines) as a function of the temperature T at $eB = 0$ for $r_A = G_A/G_S = -0.3, -0.5$ and $-0.8\,\mathrm{GeV}^2$; here, σ and μ_5 are in units of GeV. (**b**) GW spectra for $r_A = G_A/G_S = -0.3, -0.5$ and $-0.8\,\mathrm{GeV}^2$ at $eB = 0$. The figures were updated by Jingdong Shao based on the results in [67].

Table 1. Bounce solution for the nucleation temperature T_n, parameters α and $\beta/H*$ corresponding to different values of r_A and eB.

$r_A = G_A/G_S$	T_n/GeV	α	β/H_*
−0.3	0.3648	0.7343	27582
−0.5	0.2561	1.741	16274
−0.8	0.1679	4.850	6105.7

It is noticed that the value of $\beta/H*\sim10^4$ solved in this model is quite different from the typical value from that obtained in the EWPT, where the typical value of $\beta/H* = 1\sim100$ [83–85], but the holographic QCD calculations also gave $\beta/H*\sim10^4$ [62,64]. The large $\beta/H*$ indicates that the PT completes in an extremely short time period; thus, it is not favorable for the formation of the primordial black hole, as also proven in [67]. Figure 2b shows the GW spectra for $r_A = G_A/G_S = -0.3, -0.5$ and $-0.8\,\mathrm{GeV}^2$ at $eB = 0$. The GW spectra from the FOPT of the chirality imbalance can be detected by Taiji, Lisa, and DECIGO.

There are also many other models: for example, the bag model has been investigated in the early universe [86,87]. For the QCD epoch in the early universe after the EWPT in the temperature region of 100 MeV$\sim$100 GeV, we need to consider the interplay between the quark dynamics including both light flavors and heavy flavors and gluodynamics; for that purpose, the holographic QCD method might be one of the powerful theoretical tools [88–91].

3. Dense QCD Matter

Exploring the QCD phase structure and equation of state (EoS) at high baryon density have been boosted both by neutron star (NS) and heavy-ion collisions.

The search for the QCD CEP at finite baryon density has been one of the most-important goals for the BES program for RHICs, as well as for the future accelerator facilities at the FAIR and NICA. The higher-order fluctuations of conserved charges, especially the baryon number fluctuations, carry the divergence feature of the correlation length at the CEP [92,93]. The measurement of the kurtosis of the baryon number fluctuations $\kappa\sigma^2$ or C_4/C_2 from BES-I for RHICs in the collision energy $\sqrt{s_{NN}} = 200\sim7.7$ GeV shows a non-monotonic energy-dependent behavior [94–96]. It has been observed that $\kappa\sigma^2$ of the net proton number distributions starts from about 1 at $\sqrt{s_{NN}} = 200$ GeV, corresponding to the baryon chemical potential $\mu_B\sim0.1$ GeV, decreases to around 0.1 at $\sqrt{s_{NN}} = 20$ GeV, and rises quickly up to 3.5 at $\sqrt{s_{NN}} = 7.7$ GeV, corresponding to the baryon chemical potential $\mu_B\sim0.4$ GeV.

The three-flavor realistic PNJL (rPNJL) model, which takes into account eight-quark interaction [97], can give a realistic critical temperature $T_c = 160$ MeV at $\mu = 0$, and the effective potential takes the form of

$$\begin{aligned}\Omega &= g_S\sum_f\sigma_f^2 - \frac{g_D}{2}\sigma_u\sigma_d\sigma_s + 3\frac{g_1}{2}(\sum_f\sigma_f^2)^2 + 3g_2\sum_f\sigma_f^4 - 6\int_0^\Lambda\frac{d^3p}{(2\pi)^3}E_f\\ &\quad -2T\int\frac{d^3p}{(2\pi)^3}\ln[1+3(\Phi+\bar{\Phi}e^{-(E_f-\mu_f)/T})e^{-(E_f-\mu_f)/T}+e^{-3(E_f-\mu_f)/T}]\\ &\quad -2T\int\frac{d^3p}{(2\pi)^3}\ln[1+3(\Phi+\bar{\Phi}e^{-(E_f+\mu_f)/T})e^{-(E_f+\mu_f)/T}+e^{-3(E_f+\mu_f)/T}]\\ &\quad +U'(\Phi,\bar{\Phi},T). \end{aligned} \tag{2}$$

where $f = u, d, s$ refers to three-flavor light quarks, $\sigma_f = \left\langle\bar{\psi}_f\psi_f\right\rangle$ is the quark–antiquark condensate for different flavors, and $E_f = \sqrt{p^2+M_f^2}$ with M_f the constituent quark mass taking the form of $M_f = m_f - 2g_S\sigma_f + \frac{g_D}{4}\sigma_{f+1}\sigma_{f+2} - 2g_1\sigma_f(\sum_{f'}\sigma_{f'}^2) - 4g_2\sigma_f^3$. U' takes the form of $\frac{U'}{T^4} = \frac{U}{T^4} - \kappa\ln[J(\Phi,\bar{\Phi})]$ and its detailed description can be found in [98,99].

The three-flavor rPNJL model [97] predicts that the CEP of the chiral phase transition is located at $(\mu_B^E = 720$ MeV, $T^E = 93$ MeV) [99,100]. The chiral phase transition boundary in this rPNJL model is close to the extracted freeze-out line from heavy-ion collisions [101,102], and the kurtosis of baryon number fluctuations $\kappa\sigma^2$ calculated in the rPNJL model along the experimental freeze-out line [101,102] agrees well with the BES-I measurement and predicts a peak structure around $\sqrt{s_{NN}} = 5$ GeV; see Figure 3. It was emphasized in [99,100] that the dip structure of $\kappa\sigma^2$ can be explained at the low-baryon-density region, the freeze-out

line lies above the chiral phase transition line and crosses the chiral phase transition line, while the peak of $\kappa\sigma^2$ is a clean signature for the existence of the CEP.

Recently, the results at $\sqrt{s_{NN}} = 3$ GeV and the measurement of HADES at $\sqrt{s_{NN}} = 2.4$ GeV were updated in [103]. The data indicate a peak structure $\sqrt{s_{NN}} = 5$ GeV, and more data with higher precision are expected at lower collision energies. It is noted that the data at $\sqrt{s_{NN}} = 3$ GeV have the tendency to be negative, which might indicate another CEP of the liquid–gas phase transition.

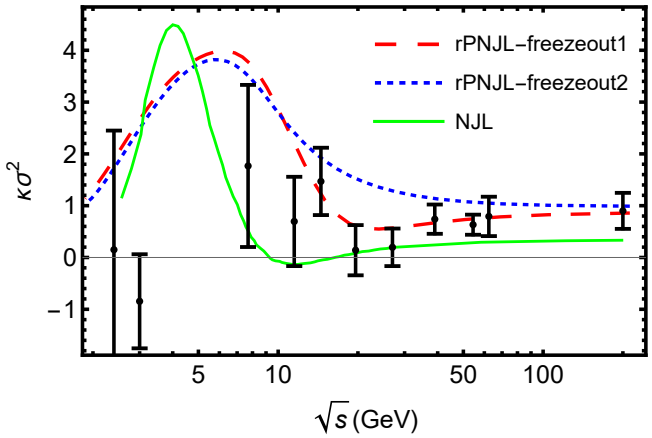

Figure 3. The $\kappa\sigma^2$ produced in the rPNJL model [99,100], as well as in the NJL model [104] as a function of $\sqrt{s}$ along the freeze-out lines, compared with the updated measurement of $C4/C2$ or $\kappa\sigma^2$ for the proton and net-proton at the RHIC BES-II program in [103]. The figure was updated by Kun Xu based on the results in [99,100].

Dense QCD matter may exist inside the neutron star (NS), which is the remnant after a massive super-giant star collapses. In 1967, the discovery of radio pulsars confirmed the existence of NSs. Since then, more than 2700 radio pulsars have been detected. From the experimental side, the mass and radius of the NSs can be measured with high precision [105–115]. Recent developments in observational astronomy including the operating satellites, the Neutron star Interior Composition Explorer (NICER), and along with the observation of the GWs, the Advanced LIGO, Virgo, and KAGRA [116,117] have also provided high precision measurements on neutron star masses and radii from the tidal deformability measurements. These high precision measurement gives very strict constraints on the equation of state (EoS) of dense QCD matter inside neutron stars.

The baryon number density n_B in the core of the NS can reach 5∼10 times of the nuclear saturation density n_s, which lies in nonperturbative QCD region. From theory side, it is quite challenging to explore the internal structure of NSs. There have been many efforts trying to describe the EoS of cold QCD dense matter including nuclear matter and quark matter by using effective models. In recent years, holographic QCD method has been applied in describing nonperturbative QCD physics. In Ref. [118], the hybrid EoS of the cold strong interaction matter has been constructed using holographic models. In the low baryon number density n_B range, Hebeler-Lattimer-Pethick-Schwenk (HLPS) can be used to describe the nuclear matter EoS. At the intermediate n_B region, the holographic QCD is used to calculate the EoS. Our holographic QCD model consists of the Einstein-Maxwell-dilaton (EMD) system for the gluodynamical background and the improved Karch-Katz-Son-Stephanov (KKSS) action for the flavor part to describe the holographic nuclear matter and the holographic quark matter. In the framework of the Einstein-Maxwell-dilaton (EMD) system, i.e., the gravity-dilaton coupling system at zero chemical potential extended to finite chemical potential. The total action of the 5-dimensional holographic QCD model is

$$S^s_{\text{total}} = S^s_{EMD} + S^s_f, \tag{3}$$

where S^s_{EMD} is the action for the EMD system in the string frame, and S^s_f is the action that describes the flavor part in the string frame. In order to investigate the equation of state, it is more convenient to work in the Einstein frame. By using the relation $g^s_{MN} = e^{\frac{4}{3}\Phi} g^E_{MN}$, the EMD background action in the Einstein frame has the form of

$$S^E_{EMD} = \frac{1}{2\kappa_5^2}\int d^5x\sqrt{-g^E}\Big[R^E - \frac{4}{3}g^{EMN}\partial_M\Phi\partial_N\Phi - V^E(\Phi) - \frac{h(\Phi)}{4}g^{EM\tilde{M}}g^{EN\tilde{N}}F_{MN}F_{\tilde{M}\tilde{N}}\Big], \tag{4}$$

with $V^E = e^{\frac{4}{3}\Phi}V^s$. The flavor part or the matter part is given by the meson part and baryon part $S^s_f = S^s_{\text{mesons}} + S^s_{\text{baryons}}$. It is expected that S^s_{baryons} is small, and the meson part can be described by the KKSS model [119]:

$$S^s_f = -\beta\int d^5x\sqrt{-g^s}e^{-\Phi}\Big\{|D_MX|^2 + V^s_X(X_M) + \frac{1}{4g_5^2}\Big(F_L^2 + F_R^2\Big)\Big\}, \tag{5}$$

where X is the 5-dimensional scalar field. In the holographic model, we take the dilation field $\phi(z) = c_1z^2$, and the function $h_\phi(z) = e^{c_2z^2 - A_E(z)}$, with $c_1 = 1.536\,\text{GeV}^2$ and $c_2 = 1.16\,\text{GeV}^2$. The 5-dimensional Newtonian constant is taken as $G_5 = 17.930$.

The hybrid model gives the mass-radius relation and the tidal deformability of the neutron stars which are in agreement with astrophysical measurements as shown in Figure 4a,b. The possible maximum mass for the neutron star is about $2.5M_\odot$ and the radius is about 12 km. In the current holographic model, we didn't consider the phase transition between the nuclear matter and the quark matter. The holographic nuclear matter here might refer to the quarkyonic phase [120,121], which is in confinement with chiral symmetry restoration.

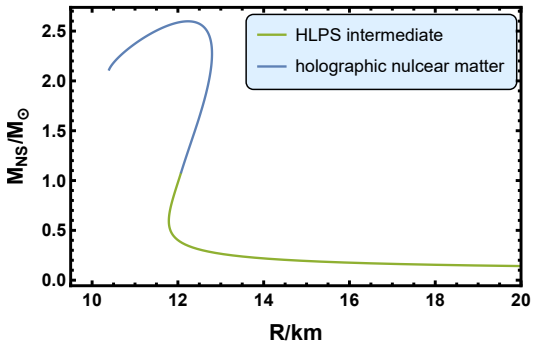

(**a**)

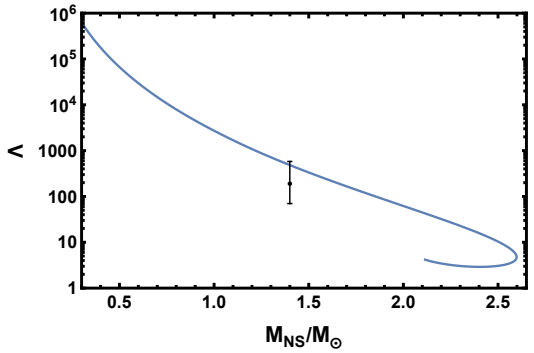

(**b**)

Figure 4. The mass-radius relation in (**a**) and tidal deformability as a function of the mass ratio between the neutron star and the sun in (**b**) calculated in a dynamical holographic QCD model. The figures are updated by Lin Zhang based on results in [118].

4. QCD Matter under Electromagnetic and Vortical Field

The hot and dense matter created in non-central heavy-ion collisions (HICs) shows the fastest rotation with the angular momentum in the range of $\mathcal{O}(10^4)\hbar$–$\mathcal{O}(10^5)\hbar$ or a vorticity of order 10^{21} s^{-1}[33,122–124], and the strongest magnetic field $B\sim10^{18}G$ for RHICs, while $B\sim10^{20}G$ at the LHC [30,31]. Both the magnetic field and rotation will polarize quarks and gluons, thus changing the QCD matter properties under an external magnetic field and rotation.

The novel phenomena of QCD matter under external magnetic fields include the chiral magnetic effect (CME) [75–77], a magnetic field enhancing the chiral symmetry breaking in the vacuum, which is called magnetic catalysis (MC) [125–127], and the critical temperature of the chiral phase transition decreasing with external magnetic fields, i.e., inverse magnetic catalysis (IMC) [128–130]. Recent lattice calculations showed some unexpected properties of pion mass under a magnetic field: (1) the neutral pion mass decreases with the magnetic field, then saturates with a strong magnetic field; (2) the charged pion mass exhibits a nonmonotonic magnetic-field-dependent behavior [131]; it first increases and reaches a peak around $eB\sim0.5\,\mathrm{GeV}^2$, then decreases. Besides, the lattice calculation also showed that the magnetic susceptibility of quark matter is negative (diamagnetism) at a low temperature and is positive (paramagnetism) at a high temperature [132,133]. Much effort has been made to understand these properties, and it is still challenging to describe all these phenomena within one self-consistent framework.

The global polarization of Λ and $\bar{\Lambda}$ was predicted in [34] and was observed by the STAR Collaboration for Au+Au collisions at $\sqrt{s_{NN}} = 7.7$–$200\,\mathrm{GeV}$ [35]. The experimental data showed that: (1) both the global spin polarization and the splitting of $P_{\Lambda/\bar{\Lambda}}$ become stronger at lower collision energy; (2) the polarization of $\bar{\Lambda}$ is larger than that of Λ, i.e., $P_{\bar{\Lambda}} > P_{\Lambda}$.

In [134], it was found that the global polarization of $\Lambda/\bar{\Lambda}$ can be induced by the rotation and the splitting of the $\Lambda-\bar{\Lambda}$ polarization induced by a magnetic field. In [134], the three-flavor NJL model included the 't Hooft determinant term with the Lagrangian $\mathcal{L}_\chi$:

$$\mathcal{L}_\chi = \frac{G_S}{2}\sum_{a=0}^{8}\Big\{(\bar{\psi}\lambda^a\psi)^2 + (\bar{\psi}i\gamma^5\lambda^a\psi)^2\Big\} - G_K\Big\{\det\bar{\psi}(1+\gamma^5)\psi + \det\bar{\psi}(1-\gamma^5)\psi\Big\}, \quad (6)$$

taking into account the anomalous magnetic moment (AMM) of quarks under an external magnetic field B:

$$\mathcal{L}_{AMM} = \bar{\psi}\Big(i\gamma^\mu D_\mu - \hat{m} + \kappa qB\sigma^{12}\Big)\psi, \quad (7)$$

and considering the contribution of the axial vector interaction under rotation characterized by the angular velocity Ω:

$$\mathcal{L}_A = \bar{\psi}\Big[\gamma^0(i\partial_t + \Omega\hat{J}_z) + \mu\gamma^0\Big]\psi - G_A\Big\{(\bar{\psi}\gamma^\mu\psi)^2 + (\bar{\psi}\gamma^\mu\gamma^5\psi)^2\Big\}. \quad (8)$$

With the values of Ω and eB extracted from experimental measurement, we input these values into the above dynamical quark model including the axial vector interaction and AMM and re-derived the polarization of the s quark and $\bar{s}$ quark, and the results are shown in Figure 5. It was noticed that the rotation contributes the same polarization to the s and $\bar{s}$ quarks, while the magnetic field contributes a positive polarization for the $\bar{s}$ quark, while giving a negative polarization for the s quark. The splitting of the $\Lambda-\bar{\Lambda}$ polarization induced by the magnetic field includes two sources: (1) the remaining magnetic field from the evolution of the system after the collision and (2) the magnetic field induced by the vorticity [135]; this is shown in Figure 6.

However, at a collision energy below 7.7 GeV, the magnitude of the magnetic field used at freeze-out is at least 20-times smaller to induce the large splitting polarization of $P_{\Lambda/\bar{\Lambda}}$. It will be needed in the future to reanalyze the magnetic field evolution at low

collision energies where the vorticity is high; thus, the generation of the magnetic field from the vorticity [135] should be taken into account simultaneously.

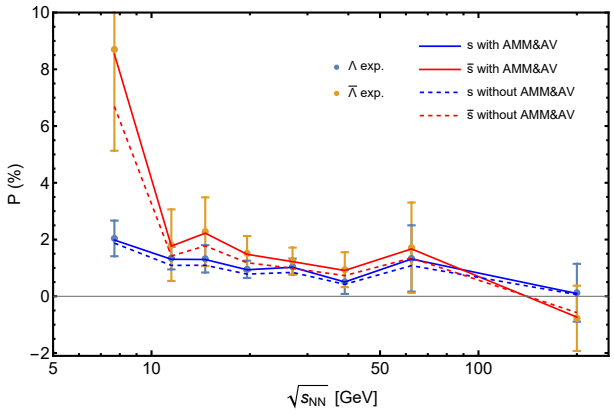

Figure 5. The spin polarization of the s quark and $\bar{s}$ quark induced by rotation and a magnetic field as a function of the collision energy $\sqrt{s}$. The figure is from [134], where the details can be found.

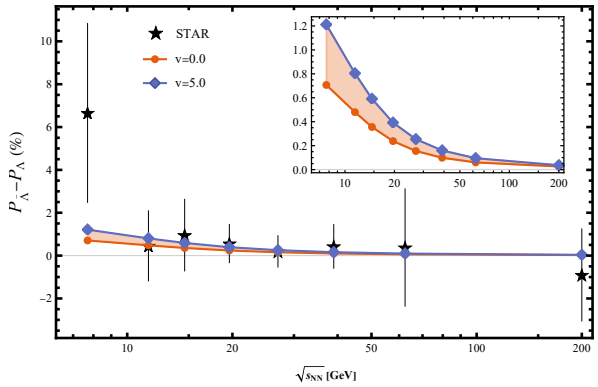

Figure 6. The splitting of $\Lambda/\bar{\Lambda}$ polarization $P_{\bar{\Lambda}} - P_{\Lambda}$ induced by rotation and a magnetic field as a function of the collision energy $\sqrt{s}$. The figure is from [134], where the details can be found.

5. Outlook

As we have shown, understanding quark matter's properties and QCD phase transitions under extreme conditions is of special interest for investigating the evolution of the universe, exploring the structure of compact stars, and understanding observable heavy-ion collisions. The properties of QCD matter and phase transitions in which we are interested lie in the nonperturbative QCD region, where the interplay of the chiral dynamics and gluodynamics plays an essential role. The lattice QCD calculation can provide first-principles results, though there are still challenges in the finite baryon density region. Four-dimensional effective QCD models, especially chiral effective models, can provide some qualitative analysis of or insight into possible interesting phenomena. Five-dimensional holographic QCD models based on the AdS/CFT correspondence have the potential to unveil the interplay of chiral dynamics and gluodynamics.

Author Contributions: These authors contributed equally to this work. All authors have read and agreed to the published version of the manuscript.

Funding: We thank Jingdong Shao, Kun Xu and LIn Zhang for the help to update the figures. This work is supported in part by NSFC Grant Nos. 12235016, 12221005, 11725523, 11735007, 11890712 and the Strategic Priority Research Program of Chinese Academy of Sciences under Grant Nos XDB34030000, the start-up funding from University of Chinese Academy of Sciences(UCAS), and the Fundamental Research Funds for the Central Universities.

Acknowledgments: We thank Jingdong Shao, Kun Xu, and Lin Zhang for the help in updating the figures.

Conflicts of Interest: The authors declare no conflict of interest.

References

1. Gross, D.J.; Wilczek, F. Ultraviolet Behavior of Nonabelian Gauge Theories. *Phys. Rev. Lett.* **1973**, *30*, 1343–1346. [CrossRef]
2. Politzer, H.D. Reliable Perturbative Results for Strong Interactions? *Phys. Rev. Lett.* **1973**, *30*, 1346–1349. [CrossRef]
3. Schwarz, D.J. The first second of the universe. *Ann. Phys.* **2003**, *12*, 220–270. [CrossRef]
4. Baym, G.; Chin, S.A. Can a Neutron Star Be a Giant MIT Bag? *Phys. Lett. B* **1976**, *62*, 241–244. [CrossRef]
5. Collins, J.C.; Perry, M.J. Superdense Matter: Neutrons Or Asymptotically Free Quarks? *Phys. Rev. Lett.* **1975**, *34*, 1353. [CrossRef]
6. Luo, X.; Wang, Q.; Xu, N.; Zhuang, P. (Eds.) *Properties of QCD Matter at High Baryon Density*; Springer: Berlin/Heidelberg, Germany, 2022. [CrossRef]
7. Karsch, F. Lattice QCD at Non-Zero Temperature and Density. 2022. Available online: http://xxx.lanl.gov/abs/2212.03015 (accessed on 30 December 2022).
8. Aarts, G.; Aichelin, J.; Allton, C.; Athenodorou, A.; Bachtis, D.; Bonanno, C.; Brambilla, N.; Bratkovskaya, E.; Bruno, M.; Caselle, M.; et al. Phase Transitions in Particle Physics–Results and Perspectives from Lattice Quantum Chromo-Dynamics. *arXiv* **2023**, arXiv:2301.04382.
9. de Forcrand, P.; D'Elia, M. Continuum limit and universality of the Columbia plot. *PoS* **2017**, *LATTICE2016*, 081. [CrossRef]
10. Karsch, F. Lattice QCD at high temperature and density. *Lect. Notes Phys.* **2002**, *583*, 209–249. [CrossRef]
11. Aoki, Y.; Endrodi, G.; Fodor, Z.; Katz, S.D.; Szabo, K.K. The Order of the quantum chromodynamics transition predicted by the standard model of particle physics. *Nature* **2006**, *443*, 675–678. [CrossRef]
12. Allton, C.R.; Ejiri, S.; Hands, S.J.; Kaczmarek, O.; Karsch, F.; Laermann, E.; Schmidt, C.; Scorzato, L. The QCD thermal phase transition in the presence of a small chemical potential. *Phys. Rev. D* **2002**, *66*, 074507, [CrossRef]
13. Allton, C.R.; Doring, M.; Ejiri, S.; Hands, S.J.; Kaczmarek, O.; Karsch, F.; Laermann, E.; Redlich, K. Thermodynamics of two flavor QCD to sixth order in quark chemical potential. *Phys. Rev. D* **2005**, *71*, 054508. [CrossRef]
14. Borsanyi, S.; Endrodi, G.; Fodor, Z.; Katz, S.D.; Krieg, S.; Ratti, C.; Szabo, K.K. QCD equation of state at nonzero chemical potential: Continuum results with physical quark masses at order mu^2. *J. High Energy Phys.* **2012**, *08*, 053. [CrossRef]
15. Bazavov, A.; Ding, H.T.; Hegde, P.; Kaczmarek, O.; Karsch, F.; Laermann, E.; Maezawa, Y.; Mukherjee, S.; Ohno, H.; Petreczky, P.; et al. The QCD Equation of State to $\mathcal{O}(\mu_B^6)$ from Lattice QCD. *Phys. Rev. D* **2017**, *95*, 054504. [CrossRef]
16. Borsányi, S.; Fodor, Z.; Guenther, J.N.; Kara, R.; Katz, S.D.; Parotto, P.; Pásztor, A.; Ratti, C.; Szabó, K.K. Lattice QCD equation of state at finite chemical potential from an alternative expansion scheme. *Phys. Rev. Lett.* **2021**, *126*, 232001. [CrossRef]
17. Pisarski, R.D.; Wilczek, F. Remarks on the Chiral Phase Transition in Chromodynamics. *Phys. Rev. D* **1984**, *29*, 338–341. [CrossRef]
18. Hatta, Y.; Ikeda, T. Universality, the QCD critical/tricritical point and the quark number susceptibility. *Phys. Rev. D* **2003**, *67*, 014028. [CrossRef]
19. Klevansky, S.P. The Nambu-Jona-Lasinio model of quantum chromodynamics. *Rev. Mod. Phys.* **1992**, *64*, 649–708. [CrossRef]
20. Zhuang, P.; Huang, M.; Yang, Z. Density effect on hadronization of a quark plasma. *Phys. Rev. C* **2000**, *62*, 054901. [CrossRef]
21. Fukushima, K. Phase diagrams in the three-flavor Nambu-Jona-Lasinio model with the Polyakov-loop. *Phys. Rev. D* **2008**, *77*, 114028; Erratum in *Phys. Rev. D* **2008**, *78*, 039902. [CrossRef]
22. Ratti, C.; Roessner, S.; Thaler, M.A.; Weise, W. Thermodynamics of the PNJL model. *Eur. Phys. J. C* **2007**, *49*, 213–217. [CrossRef]
23. Shao, G.; Tang, Z.; Gao, X.; He, W. Baryon number fluctuations and the phase structure in the PNJL model. *Eur. Phys. J. C* **2018**, *78*, 138. [CrossRef]
24. Tawfik, A. QCD phase diagram: A Comparison of lattice and hadron resonance gas model calculations. *Phys. Rev. D* **2005**, *71*, 054502. [CrossRef]
25. Redlich, K.; Karsch, F.; Tawfik, A. Heavy ion collisions and lattice QCD at finite baryon density. *J. Phys. G* **2004**, *30*, S1271–S1274. [CrossRef]
26. Tawfik, A. The Influence of strange quarks on QCD phase diagram and chemical freeze-out: Results from the hadron resonance gas model. *J. Phys. G* **2005**, *31*, S1105–S1110. [CrossRef]
27. Xin, X.y.; Qin, S.x.; Liu, Y.x. Quark number fluctuations at finite temperature and finite chemical potential via the Dyson–Schwinger equation approach. *Phys. Rev. D* **2014**, *90*, 076006. [CrossRef]
28. Fu, W.j.; Wu, Y.l. Fluctuations and Correlations of Conserved Charges near the QCD Critical Point. *Phys. Rev. D* **2010**, *82*, 074013. [CrossRef]
29. Li, Z.; Chen, Y.; Li, D.; Huang, M. Locating the QCD critical end point through the peaked baryon number susceptibilities along the freeze-out line. *Chin. Phys. C* **2018**, *42*, 013103. [CrossRef]
30. Skokov, V.; Illarionov, A.Y.; Toneev, V. Estimate of the magnetic field strength in heavy-ion collisions. *Int. J. Mod. Phys. A* **2009**, *24*, 5925–5932. [CrossRef]
31. Deng, W.T.; Huang, X.G. Event-by-event generation of electromagnetic fields in heavy-ion collisions. *Phys. Rev. C* **2012**, *85*, 044907. [CrossRef]
32. Chen, H.L.; Huang, X.G.; Liao, J. QCD phase structure under rotation. *Lect. Notes Phys.* **2021**, *987*, 349–379. [CrossRef]

33. Becattini, F.; Piccinini, F.; Rizzo, J. Angular momentum conservation in heavy-ion collisions at very high energy. *Phys. Rev. C* **2008**, *77*, 024906. [CrossRef]
34. Liang, Z.T.; Wang, X.N. Globally polarized quark-gluon plasma in non-central A+A collisions. *Phys. Rev. Lett.* **2005**, *94*, 102301; Erratum in *Phys. Rev. Lett.* **2006**, *96*, 039901. [CrossRef] [PubMed]
35. Adamczyk, L.; The STAR Collaboration. Global Λ hyperon polarization in nuclear collisions: Evidence for the most vortical fluid. *Nature* **2017**, *548*, 62–65. [CrossRef]
36. Abbott, B.P.; Abbott, R.; Abbott, T.D.; Abernathy, M.R.; Acernese, F.; Ackley, K.; Adams, C.; Adams, T.; Addesso, P.; Adhikari, R.X.; et al. Observation of Gravitational Waves from a Binary Black Hole Merger. *Phys. Rev. Lett.* **2016**, *116*, 061102. [CrossRef] [PubMed]
37. Einstein, A. Approximative Integration of the Field Equations of Gravitation. *Sitzungsber. Preuss. Akad. Wiss. Berlin (Math. Phys.)* **1916**, *1916*, 688–696.
38. Einstein, A. Über Gravitationswellen. *Sitzungsber. Preuss. Akad. Wiss. Berlin (Math. Phys.)* **1918**, *1918*, 154–167.
39. Rummukainen, K. Finite T electroweak phase transition on the lattice. *Nucl. Phys. B Proc. Suppl.* **1997**, *53*, 30–42. [CrossRef]
40. Vaskonen, V. Electroweak baryogenesis and gravitational waves from a real scalar singlet. *Phys. Rev. D* **2017**, *95*, 123515. [CrossRef]
41. Beniwal, A.; Lewicki, M.; Wells, J.D.; White, M.; Williams, A.G. Gravitational wave, collider and dark matter signals from a scalar singlet electroweak baryogenesis. *J. High Energy Phys.* **2017**, *08*, 108. [CrossRef]
42. Beniwal, A.; Lewicki, M.; White, M.; Williams, A.G. Gravitational waves and electroweak baryogenesis in a global study of the extended scalar singlet model. *J. High Energy Phys.* **2019**, *02*, 183. [CrossRef]
43. Alves, A.; Ghosh, T.; Guo, H.K.; Sinha, K.; Vagie, D. Collider and Gravitational Wave Complementarity in Exploring the Singlet Extension of the Standard Model. *J. High Energy Phys.* **2019**, *04*, 052. [CrossRef]
44. Cline, J.M.; Lemieux, P.A. Electroweak phase transition in two Higgs doublet models. *Phys. Rev.* **1997**, *D55*, 3873–3881. [CrossRef]
45. Basler, P.; Krause, M.; Muhlleitner, M.; Wittbrodt, J.; Wlotzka, A. Strong First Order Electroweak Phase Transition in the CP-Conserving 2HDM Revisited. *J. High Energy Phys.* **2017**, *02*, 121. [CrossRef]
46. Dorsch, G.C.; Huber, S.J.; Konstandin, T.; No, J.M. A Second Higgs Doublet in the Early Universe: Baryogenesis and Gravitational Waves. *J. Cosmol. Astropart. Phys.* **2017**, *1705*, 052. [CrossRef]
47. Tawfik, A.N.; Greiner, C. Early Universe Thermodynamics and Evolution in Nonviscous and Viscous Strong and Electroweak epochs: Possible Analytical Solutions. *Entropy* **2021**, *23*, 295. [CrossRef]
48. Tawfik, A.; Harko, T. Quark-Hadron Phase Transitions in Viscous Early Universe. *Phys. Rev. D* **2012**, *85*, 084032. [CrossRef]
49. Tawfik, A. Cosmological Consequences of QCD Phase Transition(s) in Early Universe. *AIP Conf. Proc.* **2009**, *1115*, 239–247. [CrossRef]
50. Tawfik, A.; Wahba, M.; Mansour, H.; Harko, T. Viscous Quark-Gluon Plasma in the Early Universe. *Annalen Phys.* **2011**, *523*, 194–207. [CrossRef]
51. Hogan, C.J. Gravitational radiation from cosmological phase transitions. *Mon. Not. R. Astron. Soc.* **1986**, *218*, 629–636. [CrossRef]
52. Kosowsky, A.; Turner, M.S.; Watkins, R. Gravitational waves from first order cosmological phase transitions. *Phys. Rev. Lett.* **1992**, *69*, 2026–2029. [CrossRef]
53. Kosowsky, A.; Turner, M.S. Gravitational radiation from colliding vacuum bubbles: Envelope approximation to many bubble collisions. *Phys. Rev. D* **1993**, *47*, 4372–4391. [CrossRef] [PubMed]
54. Kamionkowski, M.; Kosowsky, A.; Turner, M.S. Gravitational radiation from first order phase transitions. *Phys. Rev. D* **1994**, *49*, 2837–2851. [CrossRef] [PubMed]
55. Hawking, S.W.; Moss, I.G.; Stewart, J.M. Bubble Collisions in the Very Early Universe. *Phys. Rev. D* **1982**, *26*, 2681. [CrossRef]
56. Jung, T.H.; Okui, T. Primordial black holes from bubble collisions during a first-order phase transition. *arXiv* **2021**, arXiv:2110.04271.
57. Khlopov, M.Y.; Konoplich, R.; Rubin, S.; Sakharov, A.S. First order phase transitions as a source of black holes in the early universe. *arXiv* **1999**, arXiv:hep-ph/9912422.
58. Carr, B.; Clesse, S.; García-Bellido, J. Primordial black holes from the QCD epoch: Linking dark matter, baryogenesis and anthropic selection. *Mon. Not. R. Astron. Soc.* **2021**, *501*, 1426–1439. [CrossRef]
59. Byrnes, C.T.; Hindmarsh, M.; Young, S.; Hawkins, M.R.S. Primordial black holes with an accurate QCD equation of state. *J. Cosmol. Astropart. Phys.* **2018**, *08*, 041. [CrossRef]
60. Jedamzik, K. Primordial black hole formation during the QCD epoch. *Phys. Rev. D* **1997**, *55*, 5871–5875. [CrossRef] [CrossRef]
61. Profumo, S.; Ramsey-Musolf, M.J.; Shaughnessy, G. Singlet Higgs phenomenology and the electroweak phase transition. *J. High Energy Phys.* **2007**, *8*, 010. [CrossRef]
62. Chen, Y.; Huang, M.; Yan, Q.S. Gravitation waves from QCD and electroweak phase transitions. *J. High Energy Phys.* **2018**, *5*, 178. [CrossRef]
63. He, S.; Li, L.; Li, Z.; Wang, S.J. Gravitational Waves and Primordial Black Hole Productions from Gluodynamics. *arXiv* **2022**, arXiv:2210.14094.
64. Morgante, E.; Ramberg, N.; Schwaller, P. Echo of the Dark: Gravitational Waves from Dark SU(3) Yang-Mills Theory. *arXiv* **2022**, arXiv:2210.11821.

65. Asadi, P.; Kramer, E.D.; Kuflik, E.; Slatyer, T.R.; Smirnov, J. Glueballs in a thermal squeezeout model. *J. High Energy Phys.* **2022**, *7*, 006. [CrossRef]
66. Carenza, P.; Pasechnik, R.; Salinas, G.; Wang, Z.W. Glueball Dark Matter revisited. *Phys. Rev. Lett.* **2022**, *129*, 26. [CrossRef] [PubMed]
67. Shao, J.; Huang, M. Gravitational waves and primordial black holes from chirality imbalanced QCD first-order phase transition with $\mathcal{P}$ and $\mathcal{CP}$ violation. *Phys. Rev. D* **2023**, *107*, 043011. [CrossRef]
68. 't Hooft, G. Symmetry Breaking Through Bell-Jackiw Anomalies. *Phys. Rev. Lett.* **1976**, *37*, 8–11. . [CrossRef]
69. 't Hooft, G. How Instantons Solve the U(1) Problem. *Phys. Rep.* **1986**, *142*, 357–387. [CrossRef]
70. Belavin, A.A.; Polyakov, A.M.; Schwartz, A.S.; Tyupkin, Y.S. Pseudoparticle Solutions of the Yang-Mills Equations. *Phys. Lett. B* **1975**, *59*, 85–87. [CrossRef]
71. Witten, E. Current Algebra Theorems for the U(1) Goldstone Boson. *Nucl. Phys. B* **1979**, *156*, 269–283. [CrossRef]
72. Veneziano, G. U(1) Without Instantons. *Nucl. Phys. B* **1979**, *159*, 213–224. [CrossRef]
73. Vicari, E.; Panagopoulos, H. Theta dependence of SU(N) gauge theories in the presence of a topological term. *Phys. Rept.* **2009**, *470*, 93–150. [CrossRef]
74. Schäfer, T.; Shuryak, E.V. Instantons in QCD. *Rev. Mod. Phys.* **1998**, *70*, 323–426. [CrossRef]
75. Kharzeev, D.; Zhitnitsky, A. Charge separation induced by P-odd bubbles in QCD matter. *Nucl. Phys. A* **2007**, *797*, 67–79. [CrossRef]
76. Kharzeev, D.E.; McLerran, L.D.; Warringa, H.J. The Effects of topological charge change in heavy-ion collisions: 'Event by event P and CP violation'. *Nucl. Phys. A* **2008**, *803*, 227–253. [CrossRef]
77. Fukushima, K.; Kharzeev, D.E.; Warringa, H.J. The Chiral Magnetic Effect. *Phys. Rev. D* **2008**, *78*, 074033. [CrossRef]
78. Ilgenfritz, E.M.; Shuryak, E.V. Chiral Symmetry Restoration at Finite Temperature in the Instanton Liquid. *Nucl. Phys. B* **1989**, *319*, 511–520. [CrossRef]
79. Ilgenfritz, E.M.; Shuryak, E.V. Quark induced correlations between instantons drive the chiral phase transition. *Phys. Lett. B* **1994**, *325*, 263–266. [CrossRef]
80. Schäfer, T.; Shuryak, E.V.; Verbaarschot, J.J.M. The Chiral phase transition and instanton—Anti-instanton molecules. *Phys. Rev. D* **1995**, *51*, 1267–1281. [CrossRef]
81. Zhang, Z. Correction to the Chiral Magnetic Effect from axial vector interaction. *Phys. Rev. D* **2012**, *85*, 114028. [CrossRef]
82. Yu, L.; Liu, H.; Huang, M. Spontaneous generation of local CP violation and inverse magnetic catalysis. *Phys. Rev. D* **2014**, *90*, 074009. [CrossRef]
83. Ellis, J.; Lewicki, M.; No, J.M. On the Maximal Strength of a First-Order Electroweak Phase Transition and its Gravitational Wave Signal. *J. Cosmol. Astropart. Phys.* **2019**, *04*, 003. [CrossRef]
84. Leitao, L.; Megevand, A. Gravitational waves from a very strong electroweak phase transition. *J. Cosmol. Astropart. Phys.* **2016**, *05*, 037.
85. Chala, M.; Krause, C.; Nardini, G. Signals of the electroweak phase transition at colliders and gravitational wave observatories. *J. High Energy Phys.* **2018**, *07*, 062. [CrossRef]
86. DeGrand, T.A.; Kajantie, K. Supercooling, Entropy Production and Bubble Kinetics in the Quark—Hadron Phase Transition in the Early Universe. *Phys. Lett. B* **1984**, *147*, 273–278. [CrossRef]
87. Schettler, S.; Boeckel, T.; Schaffner-Bielich, J. Imprints of the QCD Phase Transition on the Spectrum of Gravitational Waves. *Phys. Rev. D* **2011**, *83*, 064030. [CrossRef]
88. Chen, Y.; Li, D.; Huang, M. The dynamical holographic QCD method for hadron physics and QCD matter. *Commun. Theor. Phys.* **2022**, *74*, 097201. [CrossRef]
89. Gursoy, U.; Kiritsis, E. Exploring improved holographic theories for QCD: Part I. *J. High Energy Phys.* **2008**, *02*, 032. [CrossRef]
90. Gursoy, U.; Kiritsis, E.; Nitti, F. Exploring improved holographic theories for QCD: Part II. *J. High Energy Phys.* **2008**, *02*, 019. [CrossRef]
91. Gubser, S.S.; Nellore, A.; Pufu, S.S.; Rocha, F.D. Thermodynamics and bulk viscosity of approximate black hole duals to finite temperature quantum chromodynamics. *Phys. Rev. Lett.* **2008**, *101*, 131601. [CrossRef]
92. Stephanov, M.A. Non-Gaussian fluctuations near the QCD critical point. *Phys. Rev. Lett.* **2009**, *102*, 032301. [CrossRef]
93. Stephanov, M.A. On the sign of kurtosis near the QCD critical point. *Phys. Rev. Lett.* **2011**, *107*, 052301. [CrossRef]
94. Adamczyk, L.; Adkins, J.K.; Agakishiev, G.; Aggarwal, M.M.; Ahammed, Z.; Alekseev, I.; Alford, J.; Anson, C.D.; Aparin, A.; Arkhipkin, D.; et al. Energy Dependence of Moments of Net-proton Multiplicity Distributions at RHIC. *Phys. Rev. Lett.* **2014**, *112*, 032302. [CrossRef] [PubMed]
95. Aggarwal, M.M.; Ahammed, Z.; Alakhverdyants, A.V.; Alekseev, I.; Alford, J.; Anderson, B.D.; Arkhipkin, D.; Averichev, G.S.; Balewski, J.; Barnby, L.S.; et al. Higher Moments of Net-proton Multiplicity Distributions at RHIC. *Phys. Rev. Lett.* **2010**, *105*, 022302. [CrossRef] [PubMed]
96. Luo, X.; Xu, N. Search for the QCD Critical Point with Fluctuations of Conserved Quantities in Relativistic Heavy-Ion Collisions at RHIC: An Overview. *Nucl. Sci. Tech.* **2017**, *28*, 112. [CrossRef]
97. Bhattacharyya, A.; Ghosh, S.K.; Maity, S.; Raha, S.; Ray, R.; Saha, K.; Upadhaya, S. Reparametrizing the Polyakov–Nambu–Jona-Lasinio model. *Phys. Rev. D* **2017**, *95*, 054005. [CrossRef]

98. Ghosh, S.K.; Mukherjee, T.K.; Mustafa, M.G.; Ray, R. PNJL model with a Van der Monde term. *Phys. Rev. D* **2008**, *77*, 094024. [CrossRef]
99. Xu, K.; Li, Z.; Huang, M. QCD critical end point from a realistic PNJL model. *EPJ Web Conf.* **2018**, *192*, 00019. [CrossRef]
100. Li, Z.; Xu, K.; Wang, X.; Huang, M. The kurtosis of net baryon number fluctuations from a realistic Polyakov–Nambu–Jona-Lasinio model along the experimental freeze-out line. *Eur. Phys. J. C* **2019**, *79*, 245. [CrossRef]
101. Das, S. Identified particle production and freeze-out properties in heavy-ion collisions at RHIC Beam Energy Scan program. *EPJ Web Conf.* **2015**, *90*, 08007. [CrossRef]
102. Begun, V.V.; Vovchenko, V.; Gorenstein, M.I. Updates to the p+p and A+A chemical freeze-out lines from the new experimental data. *J. Phys. Conf. Ser.* **2017**, *779*, 012080. [CrossRef]
103. Abdallah, M.S.; Aboona, B.E.; Adam, J.; Adamczyk, L.; Adams, J.R.; Adkins, J.K.; Agakishiev, G.; Aggarwal, I.; Aggarwal, M.M.; Ahammed, Z.; et al. Measurements of Proton High Order Cumulants in $\sqrt{s_{\rm NN}}$ = 3 GeV Au+Au Collisions and Implications for the QCD Critical Point. *Phys. Rev. Lett.* **2022**, *128*, 202303. [CrossRef]
104. Fan, W.; Luo, X.; Zong, H.S. Mapping the QCD phase diagram with susceptibilities of conserved charges within Nambu–Jona-Lasinio model. *Int. J. Mod. Phys. A* **2017**, *32*, 1750061. [CrossRef]
105. Shapiro, I.I. Fourth Test of General Relativity. *Phys. Rev. Lett.* **1964**, *13*, 789–791. [CrossRef]
106. Demorest, P.; Pennucci, T.; Ransom, S.; Roberts, M.; Hessels, J. Shapiro Delay Measurement of A Two Solar Mass Neutron Star. *Nature* **2010**, *467*, 1081–1083. [CrossRef] [PubMed]
107. Fonseca, E.; Pennucci, T.T.; Ellis, J.A.; Stairs, I.H.; Nice, D.J.; Ransom, S.M.; Demorest, P.B.; Arzoumanian, Z.; Crowter, K.; Dolch, T.; et al. The NANOGrav Nine-year Data Set: Mass and Geometric Measurements of Binary Millisecond Pulsars. *Astrophys. J.* **2016**, *832*, 167. [CrossRef]
108. Antoniadis, J.; Freire, P.C.C.; Wex, N.; Tauris, T.M.; Lynch, R.S.; van Kerkwijk, M.H.; Kramer, M.; Bassa, C.; Dhillon, V.S.; Driebe, T.; et al. A Massive Pulsar in a Compact Relativistic Binary. *Science* **2013**, *340*, 6131. . 1233232. [CrossRef] [PubMed]
109. Cromartie, H.T.; Fonseca, E.; Ransom, S.M.; Demorest, P.B.; Arzoumanian, Z.; Blumer, H.; Brook, P.R.; DeCesar, M.E.; Dolch, T.; Ellis, J.A.; et al. Relativistic Shapiro delay measurements of an extremely massive millisecond pulsar. *Nature Astron.* **2019**, *4*, 72–76. [CrossRef]
110. Fonseca, E.; Cromartie, H.T.; Pennucci, T.T.; Ray, P.S.; Kirichenko, A.Y.; Ransom, S.M.; Demorest, P.B.; Stairs, I.H.; Arzoumanian, Z.; Guillemot, L.; et al. Refined Mass and Geometric Measurements of the High-mass PSR J0740+6620. *Astrophys. J. Lett.* **2021**, *915*, L12. [CrossRef]
111. van Kerkwijk, M.H.; Breton, R.; Kulkarni, S.R. Evidence for a Massive Neutron Star from a Radial-Velocity Study of the Companion to the Black Widow Pulsar PSR B1957+20. *Astrophys. J.* **2011**, *728*, 95. [CrossRef]
112. Miller, M.C.; Lamb, F.K.; Dittmann, A.J.; Bogdanov, S.; Arzoumanian, Z.; Gendreau, K.C.; Guillot, S.; Harding, A.K.; Ho, W.C.G.; Lattimer, J.M.; et al. PSR J0030+0451 Mass and Radius from *NICER* Data and Implications for the Properties of Neutron Star Matter. *Astrophys. J. Lett.* **2019**, *887*, L24. [CrossRef]
113. Riley, T.E.; Watts, A.L.; Bogdanov, S.; Ray, P.S.; Ludlam, R.M.; Guillot, S.; Arzoumanian, Z.; Baker, C.L.; Bilous, A.V.; Chakrabarty, D.; et al. A *NICER* View of PSR J0030+0451: Millisecond Pulsar Parameter Estimation. *Astrophys. J. Lett.* **2019**, *887*, L21. [CrossRef]
114. Miller, M.C.; Lamb, F.K.; Dittmann, A.J.; Bogdanov, S.; Arzoumanian, Z.; Gendreau, K.C.; Guillot, S.; Ho, W.C.G.; Lattimer, J.M.; Loewenstein, M.; et al. The Radius of PSR J0740+6620 from NICER and XMM-Newton Data. *Astrophys. J. Lett.* **2021**, *918*, L28. [CrossRef]
115. Riley, T.E.; Watts, A.L.; Ray, P.S.; Bogdanov, S.; Guillot, S.; Morsink, S.M.; Bilous, A.V.; Arzoumanian, Z.; Choudhury, D.; Deneva, J.S.; et al. A NICER View of the Massive Pulsar PSR J0740+6620 Informed by Radio Timing and XMM-Newton Spectroscopy. *Astrophys. J. Lett.* **2021**, *918*, L27. [CrossRef]
116. Abbott, B.P.; Abbott, R.; Abbott, T.D.; Acernese, F.; Ackley, K.; Adams, C.; Adams, T.; Addesso, P.; Adhikari, R.X.; Adya, V.B.; et al. GW170817: Measurements of neutron star radii and equation of state. *Phys. Rev. Lett.* **2018**, *121*, 161101. [CrossRef] [PubMed]
117. Abbott, R.; Abbott, T.D.; Abraham, S.; Acernese, F.; Ackley, K.; Adams, C.; Adhikari, R.X.; Adya, V.B.; Affeldt, C.; Agathos, M.; et al. GW190814: Gravitational Waves from the Coalescence of a 23 Solar Mass Black Hole with a 2.6 Solar Mass Compact Object. *Astrophys. J. Lett.* **2020**, *896*, L44. [CrossRef]
118. Zhang, L.; Huang, M. Holographic cold dense matter constrained by neutron stars. *Phys. Rev. D* **2022**, *106*, 096028. [CrossRef]
119. Karch, A.; Katz, E.; Son, D.T.; Stephanov, M.A. Linear confinement and AdS/QCD. *Phys. Rev. D* **2006**, *74*, 015005. [CrossRef]
120. McLerran, L.; Reddy, S. Quarkyonic Matter and Neutron Stars. *Phys. Rev. Lett.* **2019**, *122*, 122701. [CrossRef]
121. Chen, X.; Li, D.; Hou, D.; Huang, M. Quarkyonic phase from quenched dynamical holographic QCD model. *J. High Energy Phys.* **2020**, *03*, 073. [CrossRef]
122. Deng, W.T.; Huang, X.G. Vorticity in Heavy-Ion Collisions. *Phys. Rev. C* **2016**, *93*, 064907. [CrossRef]
123. Li, H.; Pang, L.G.; Wang, Q.; Xia, X.L. Global Λ polarization in heavy-ion collisions from a transport model. *Phys. Rev. C* **2017**, *96*, 054908. [CrossRef]
124. Wei, D.X.; Deng, W.T.; Huang, X.G. Thermal vorticity and spin polarization in heavy-ion collisions. *Phys. Rev. C* **2019**, *99*, 014905. [CrossRef]
125. Klevansky, S.P.; Lemmer, R.H. Chiral symmetry restoration in the Nambu-Jona-Lasinio model with a constant electromagnetic field. *Phys. Rev. D* **1989**, *39*, 3478–3489. [CrossRef] [PubMed]

126. Klimenko, K.G. Three-dimensional Gross-Neveu model in an external magnetic field. *Teor. Mat. Fiz.* **1991**, *89*, 211–221. [CrossRef]
127. Gusynin, V.P.; Miransky, V.A.; Shovkovy, I.A. Dimensional reduction and catalysis of dynamical symmetry breaking by a magnetic field. *Nucl. Phys. B* **1996**, *462*, 249–290. [CrossRef]
128. Bali, G.S.; Bruckmann, F.; Endrodi, G.; Fodor, Z.; Katz, S.D.; Krieg, S.; Schafer, A.; Szabo, K.K. The QCD phase diagram for external magnetic fields. *J. High Energy Phys.* **2012**, *02*, 044. [CrossRef]
129. Bali, G.S.; Bruckmann, F.; Endrodi, G.; Fodor, Z.; Katz, S.D.; Schafer, A. QCD quark condensate in external magnetic fields. *Phys. Rev. D* **2012**, *86*, 071502. [CrossRef]
130. Bali, G.S.; Bruckmann, F.; Endrodi, G.; Gruber, F.; Schaefer, A. Magnetic field-induced gluonic (inverse) catalysis and pressure (an)isotropy in QCD. *J. High Energy Phys.* **2013**, *04*, 130. [CrossRef]
131. Ding, H.T.; Li, S.T.; Mukherjee, S.; Tomiya, A.; Wang, X.D. Meson masses in external magnetic fields with HISQ fermions. *PoS* **2020**, *LATTICE2019*, 250. [CrossRef]
132. Bali, G.S.; Bruckmann, F.; Constantinou, M.; Costa, M.; Endrodi, G.; Katz, S.D.; Panagopoulos, H.; Schafer, A. Magnetic susceptibility of QCD at zero and at finite temperature from the lattice. *Phys. Rev. D* **2012**, *86*, 094512. [CrossRef]
133. Bali, G.S.; Endrődi, G.; Piemonte, S. Magnetic susceptibility of QCD matter and its decomposition from the lattice. *J. High Energy Phys.* **2020**, *07*, 183. [CrossRef]
134. Xu, K.; Lin, F.; Huang, A.; Huang, M. Λ/Λ^{-} polarization and splitting induced by rotation and magnetic field. *Phys. Rev. D* **2022**, *106*, L071502. [CrossRef]
135. Guo, X.; Liao, J.; Wang, E. Spin Hydrodynamic Generation in the Charged Subatomic Swirl. *Sci. Rep.* **2020**, *10*, 2196. [CrossRef] [PubMed]

Disclaimer/Publisher's Note: The statements, opinions and data contained in all publications are solely those of the individual author(s) and contributor(s) and not of MDPI and/or the editor(s). MDPI and/or the editor(s) disclaim responsibility for any injury to people or property resulting from any ideas, methods, instructions or products referred to in the content.